

## *Supporting Information*

### **Time-Resolved Radioluminescence of the Cu(I) Cluster $\text{Cu}_4\text{I}_6^{2-}$ . Different responses to Photo, X-ray, $\beta$ -ray and $\alpha$ -ray Excitation**

John V. Garcia, Camilo Guzman, Alexander A. Mikhailovsky, Sean Devitt, James R. Tinsley, John A. DiBenedetto, and Peter C. Ford

#### **Table of Contents:**

#### **Figures:**

- Figure S1** PL and RL spectra of compound **I**.
- Figure S2** PL excitation spectra for compounds **I** and **II**.
- Figure S2** Diffuse reflectance spectra of compounds **I** and **II**.
- Figure S3** Emission spectra of compound **I** under 270 and 370 nm excitation.
- Figure S4** PL spectrum of solid **II**.
- Figure S5** PL lifetime measurements for solid compound **II** at ambient temperature.
- Figure S6** TRRL decay from **II** upon pulsed X-ray excitation.
- Figure S7** Temporal RL spectra of solid **I** recorded using a 50 ns gate.
- Figure S8** Temporal RL spectra from solid **II** after pulsed X-ray excitation.
- Figure S9** TRRL decay from solid compound **II** after  $\beta$ -ray excitation
- Figure S10** TRRL decay from solid compound **II** after  $\alpha$ -particle excitation.
- Figure S11** Double exponential fits of X-ray TRRL data for **I** and **II**.
- Figure S12** Double exponential fits of  $\beta$ -ray TRRL data for **I** and **II**.
- Figure S13** Double exponential fits of  $\alpha$ -particle TRRL data for **I** and **II**.
- Figure S14** UCSB apparatus used to record X-ray radioluminescence spectra.
- Figure S15** Time-resolved X-Ray scintillation spectrometer assembled for generating TRRL spectra.
- Figure S16** The STL Fluor Decay System based on time-correlated single photon counting.

#### **Schemes**

- Scheme S1** Models for fitting the emission decay behavior from high energy radiation excitation.

#### **Experimental Methods**

##### **Materials:**

##### **Synthesis of copper compounds**

##### **Photophysical methods**

##### **Radioluminescence techniques**

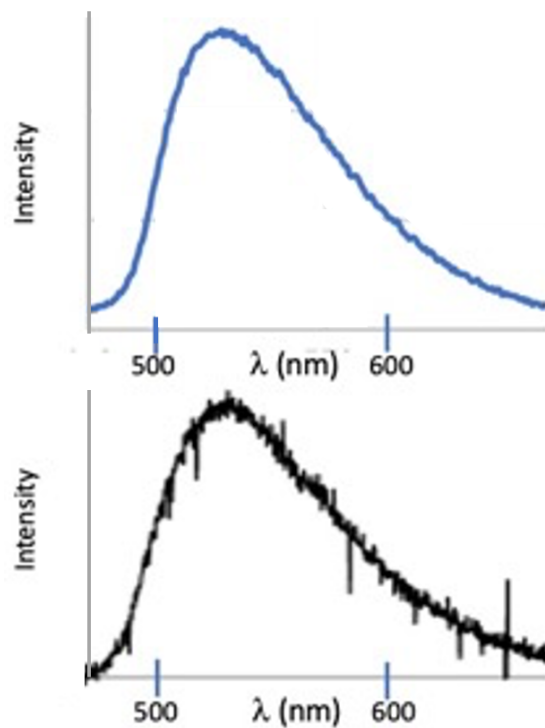


**Figure S1:** *Top:* PL spectrum of crystalline  $[\text{Na}_2(18\text{-crown-6})_2(\text{H}_2\text{O})_3][\text{Cu}_4\text{I}_6]$  (**I**) using 450 nm excitation. *Bottom:* RL spectrum of solid **I** at ambient temperature using a continuous X-ray excitation source (40 kV, 30 mA)- see Experimental. (The positive and negative spikes are shot noise artifacts that also appear with a blank sample.)

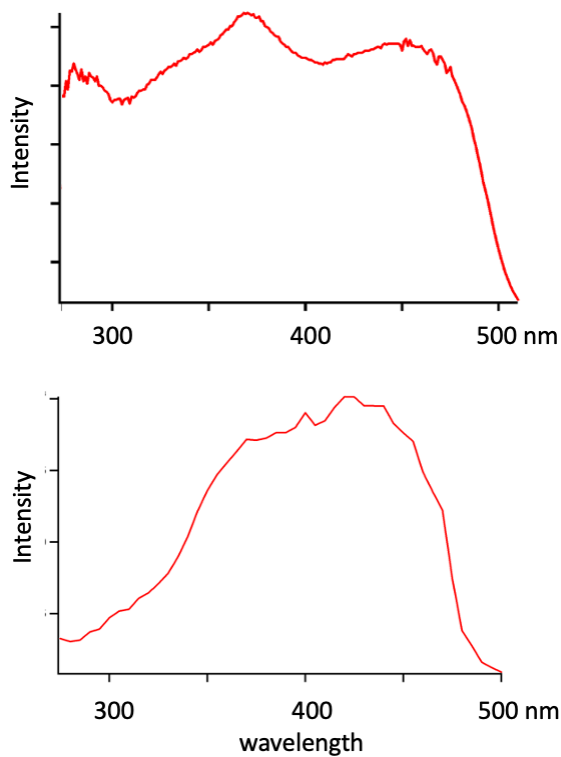


**Figure S2.** Excitation spectra of the solid compounds **I** (top) and **II** (bottom) monitored at 535 nm in each case.

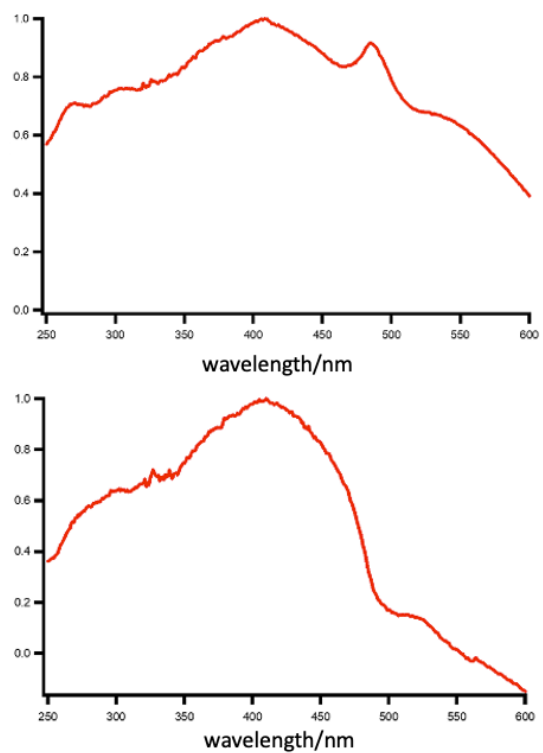


**Figure S3.** Normalized diffuse reflectance spectra of compounds **I** (top) and **II** (bottom).

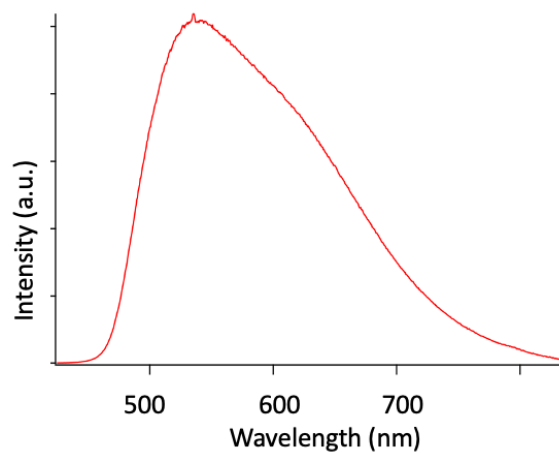


**Figure S4.** PL spectrum of solid  $[\text{Li}_2(\text{benzo-15-crown-5})_2(\text{H}_2\text{O})_3][\text{Cu}_4\text{I}_6]$  (**II**) in a thin quartz cell recorded with 290 nm excitation and showing the  $\lambda_{\text{max}}^{\text{em}} = 535$  nm.

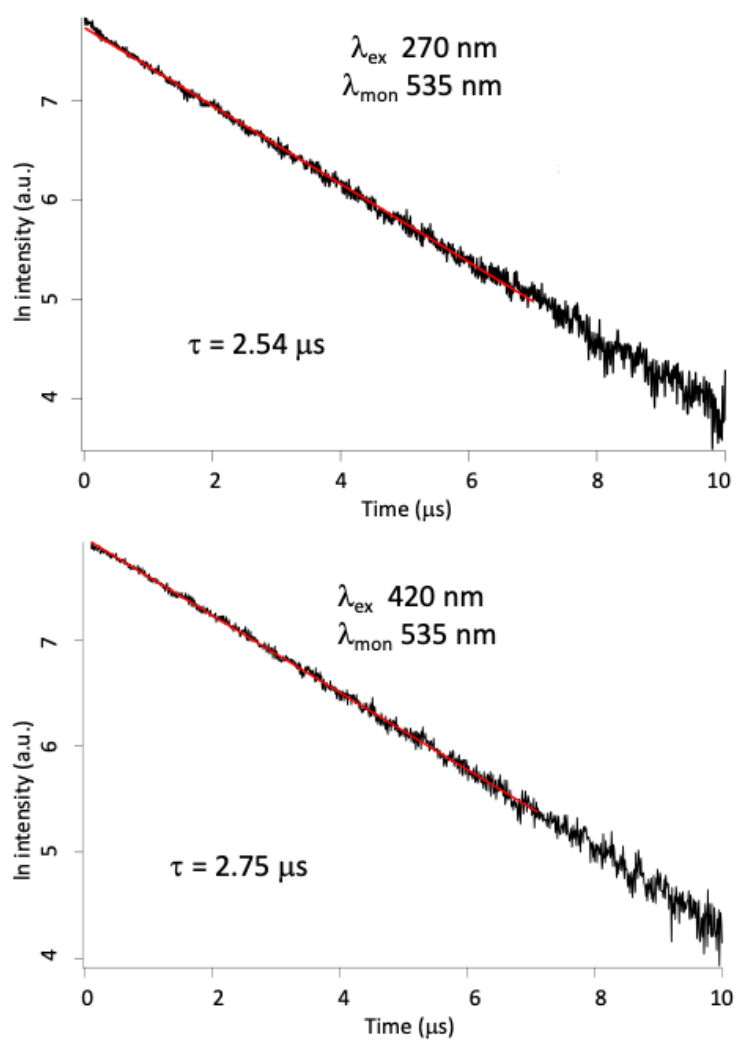


**Figure S5. Top:** PL decay of **II** after pulsed laser excitation at 270 nm monitored at 535 nm and data collected at 10 ns intervals. The red line shows the fit to single exponential decay with  $\tau_{\text{PL}} = 2.54 \mu\text{s}$ . **Bottom:** PL decay of **II** after pulsed laser excitation at 420 nm monitored at 535 nm and data collected at 10 ns intervals. The red line shows the fit to single exponential decay with  $\tau_{\text{PL}} = 2.75 \mu\text{s}$ .

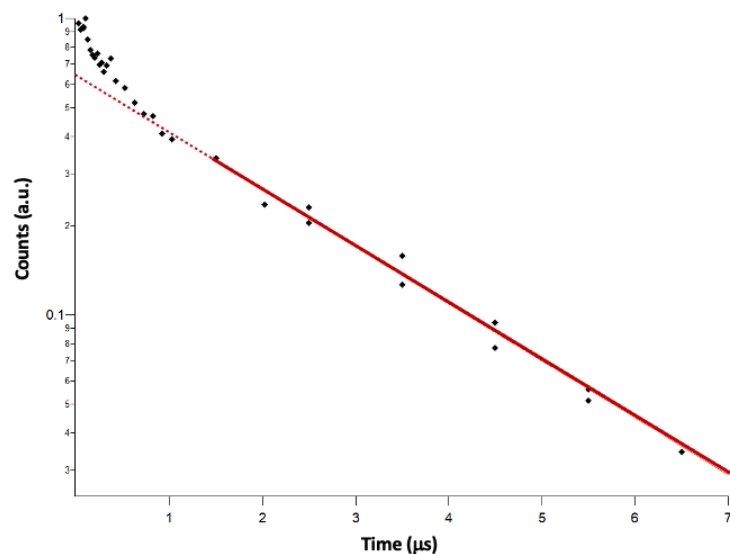


**Figure S6.** Log plot of the integrated RL intensity as a function of the delay time from the pulsed X-ray excitation (150 KeV) of crystalline **II**. The solid line is the exponential fit of the data from 1.5 to 7  $\mu\text{s}$  giving a slope ( $-k_d$ ) of  $-0.441 \mu\text{s}^{-1}$ .  $\tau_{\text{RL}} = 1/k_d = 2.27 \mu\text{s}$ . The dotted line is a simple extension of that line to  $t=0$ . The departure from mono-exponential behavior at the shorter time frame is quite evident.

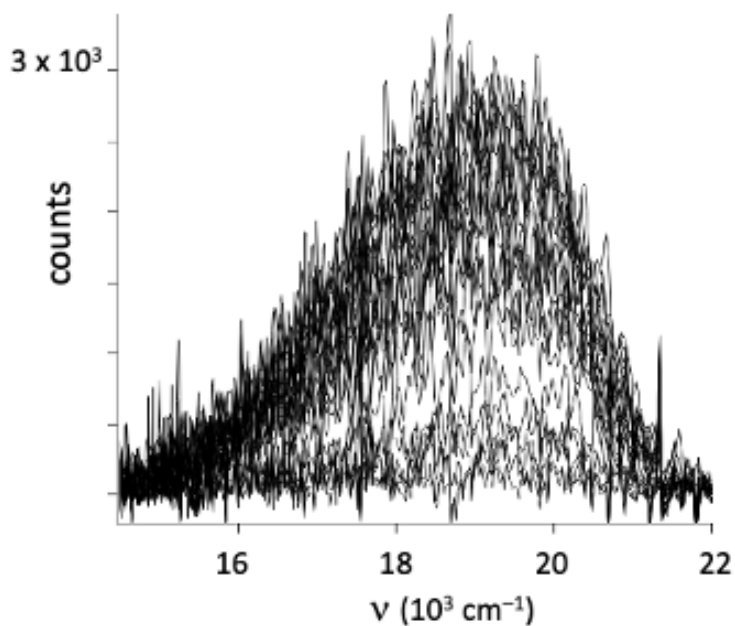


**Figure S7.** Temporal RL spectra of solid **I** recorded using a 50 ns gate at 25 ns intervals initially after pulsed X-ray excitation. The higher noise is due to the small signal owing to the narrow gate width. These are the spectral data used to construct Figure 2b.

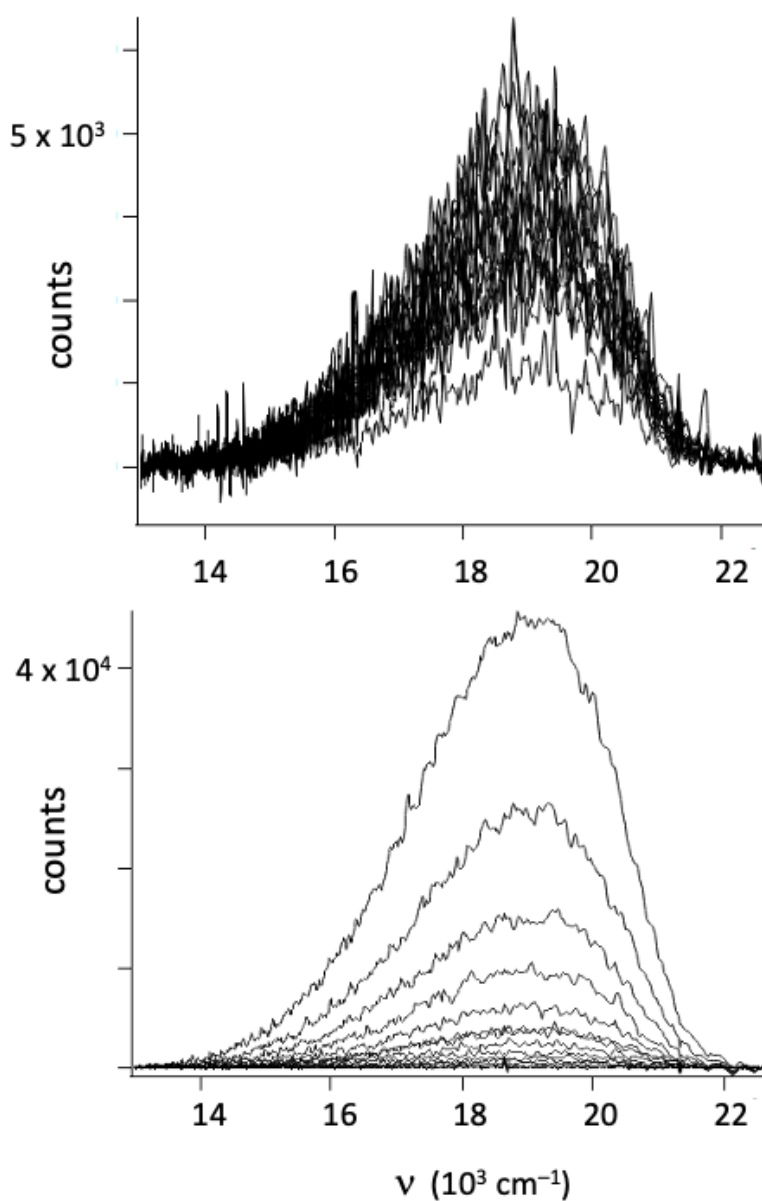


**Figure S8. Bottom:** Temporal RL spectra of solid **II** recorded using a 1  $\mu\text{s}$  gate at 1  $\mu\text{s}$  intervals after pulsed x-ray excitation. The first spectrum was measured with no delay. **Top:** Temporal RL spectra of solid **II** recorded using a 50 ns gate at different time intervals after pulsed x-ray excitation (these intervals were 0, then every 25 ns to 300 ns, then every 100 ns to 1  $\mu\text{s}$ . The last spectrum was recorded at 2  $\mu\text{s}$ . The higher noise is due to the smaller signal owing the much narrower gate width.

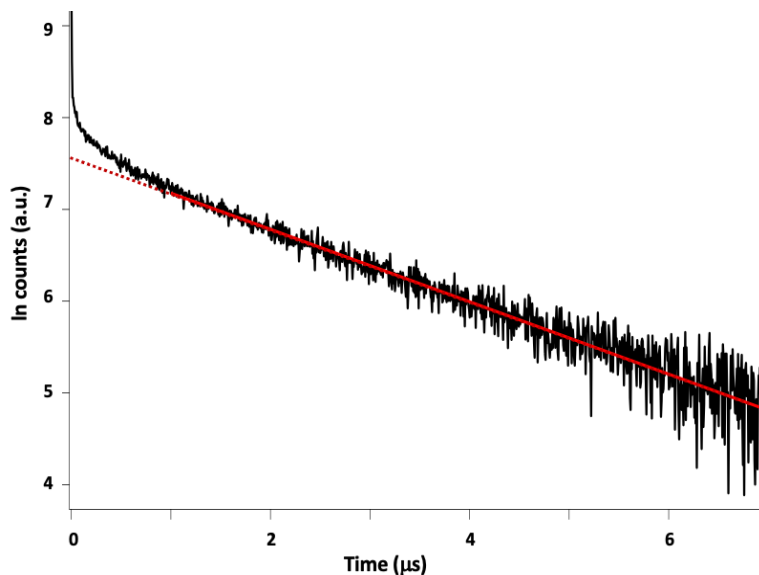


**Figure S9.** Single photon counting measurement of the time dependent radioluminescence from solid compound **II** (single crystal) using the FDS (see Experimental section) with  $\beta$ -particle excitation from a  $^{90}\text{Sr}$  radiation source. *Solid red line:*  $\ln(\text{counts})$  plot of the scintillation data for the longer time frame (1-7  $\mu\text{s}$ ) showing an exponential RL decay with a lifetime of 2.53  $\mu\text{s}$ . *Red dotted line:* linear extension of the  $\ln(\text{counts})$  versus time data to emphasize departure from exponential decay in the early stages.

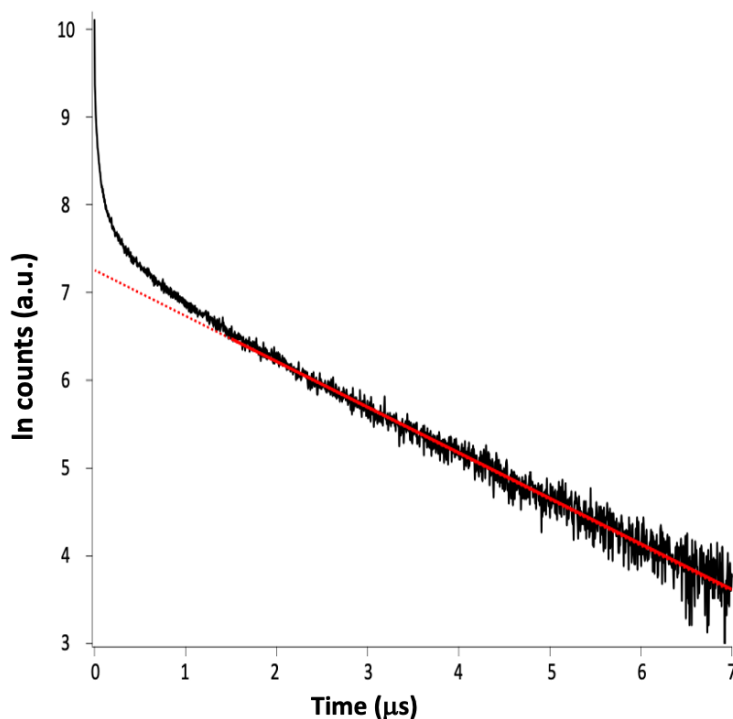


**Figure S10.** Single photon counting measurement of the time dependent radioluminescence from solid compound **II** (single crystal) using the FDS (see Experimental section) with  $\alpha$ -particle excitation from a  $^{244}\text{Cm}$  source. *Solid red line:* the  $\ln(\text{counts})$  plot of the scintillation data consistent with exponential RL decay with a lifetime of 1.93  $\mu\text{s}$  for the longer time frame (1.5-7  $\mu\text{s}$ ). *Red dotted line:* linear extension of the  $\ln(\text{counts})$  versus time data to emphasize departure from exponential decay in the early stages.

**Scheme S1.** Models for fitting the emission decay behavior from high energy radiation excitation.

*Model 1:* Fitting the excited state decay to a kinetics model involving both unimolecular deactivation and bimolecular annihilation:

The rate law for this model is:

$$-\frac{d[I_{CC}]}{dt} = k_d [I_{CC}] + k_q [I_{CC}]^2 \quad (S1)$$

where the intensity  $[I_{CC}]$  of emission from the cluster centered excited state  $CC^*$  is assumed to be proportional to the concentration of that excited state,  $k_d$  is the rate constant for unimolecular deactivation from  $CC^*$  and is the inverse of the emission lifetime ( $k_d = \tau^{-1}$ ) determined at the longer time frame ( $> 2 \mu s$ ) for each excitation source, and  $k_q$  is the bimolecular quenching constant in the medium. The approximate solution to the differential equation would be:

$$[I_{CC}]_t = -\frac{k_d * e^{C*k_d}}{k_q * e^{C*k_d} - e^{k_d*t}} \quad (S2)$$

where C equals

$$C = -\frac{1}{k_d} * \ln \left( \frac{k_d + k_q * [I_{CC}]_0}{[I_{CC}]_0} \right) \quad (S3)$$

and  $[I_{CC}]_0$  is the emission intensity at  $t = 0$

Attempts to fit the data used to plot the data in Figures 2b, 2c and 2d and SI Figs S6, S9 & S10 using eq. S2 gave very unsatisfactory fits. This was not surprising given that Eq. S1 does not take into account a mechanism where there would be multiple  ${}^3CC^*$  excited states at varied, but fixed, distances from each other in the solid. As a result,  $k_q$  is not a constant but would depend (exponentially) on the distance between respective ES (assuming the Dexter mechanism for energy transfer). Another potential complication would be exciton migration within the crystal, if such migration occurs on a relevant time scale. Lastly, the distribution of the multiple excited molecules resulting from the interaction of the high energy particles with these cuprous crystals will not be homogenous. Thus, Monte Carlo simulation may be the best approach to modelling the temporal RL; however, such analysis is outside the scope of this communication.

*Model 2: Double exponential fits:*

$$[I_{CC}] = [I_{CC}]_0 * (A_1 e^{-k_1 t} + A_2 e^{-k_d t}). \quad (S4)$$

Better fits (Figs. S11-S12) were obtained for the temporal X-ray and beta-ray excitation data using a double exponential model (eq. S4) with  $k_d$  having the same definition as above; however, This model did not give a very good fit for the alpha-particle excitation (Fig S-13). Regardless, it is unclear what physical model a fit to the double exponential would represent.

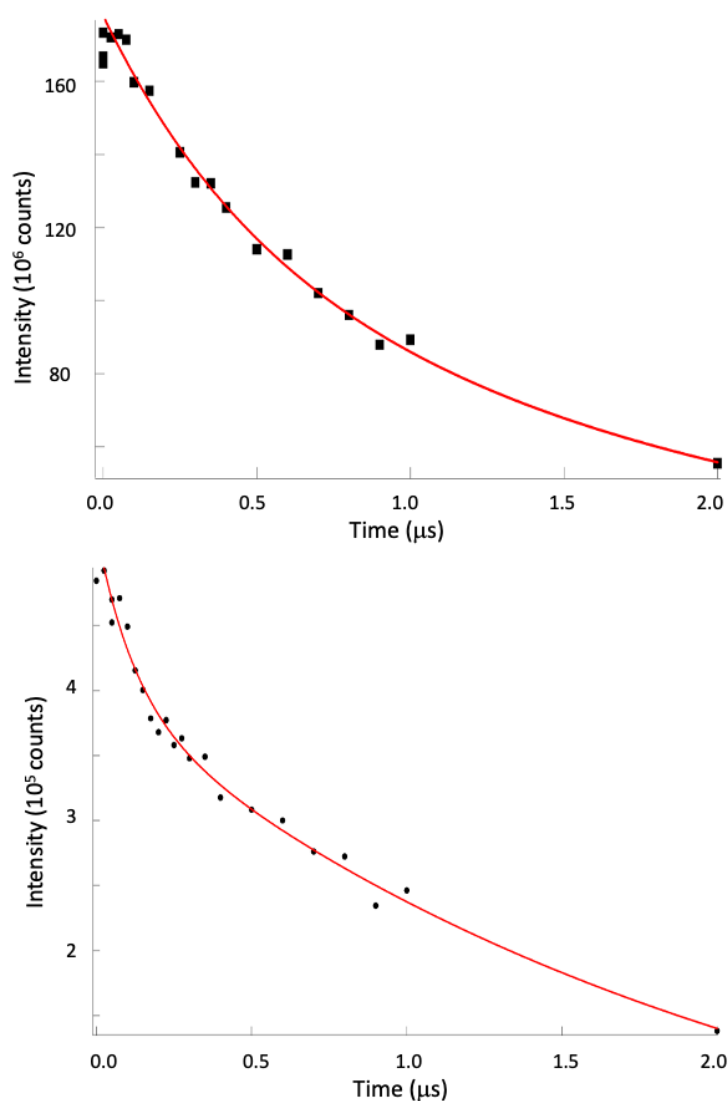


**Figure S11.** Double exponential fits ( $\text{Intensity} = I_0(A_1e^{k_1t} + A_2e^{k_2t})$ ) of scintillation responses to the X-ray excitation of compound **I** and **II** over the range 0 to 2  $\mu\text{s}$ , where  $I_0$  is the scintillation intensity at  $t=0$ . In each case,  $k_2$  was fixed as the value derived from the fit of the emission data from 2  $\mu\text{s}$  to 7  $\mu\text{s}$  for X-ray excitation of the respective compounds (Figs. 4 and S6). **Top:** Compound **I**. The fit gave the values:  $A_1 = 663 \pm 313$ ,  $k_1 = 1.98 \pm 1.3 \mu\text{s}^{-1}$ ,  $A_2 = 969 \pm 530$ , and  $k_2$  was fixed at  $0.444 \mu\text{s}^{-1}$ . **Bottom:** Compound **II**. The fit gave the values:  $A_1 = 105 \pm 12$ ,  $k_1 = 8.3 \pm 0.02 \mu\text{s}^{-1}$ ,  $A_2 = 409 \pm 33$ , and  $k_2$  was fixed at  $0.476 \mu\text{s}^{-1}$ .

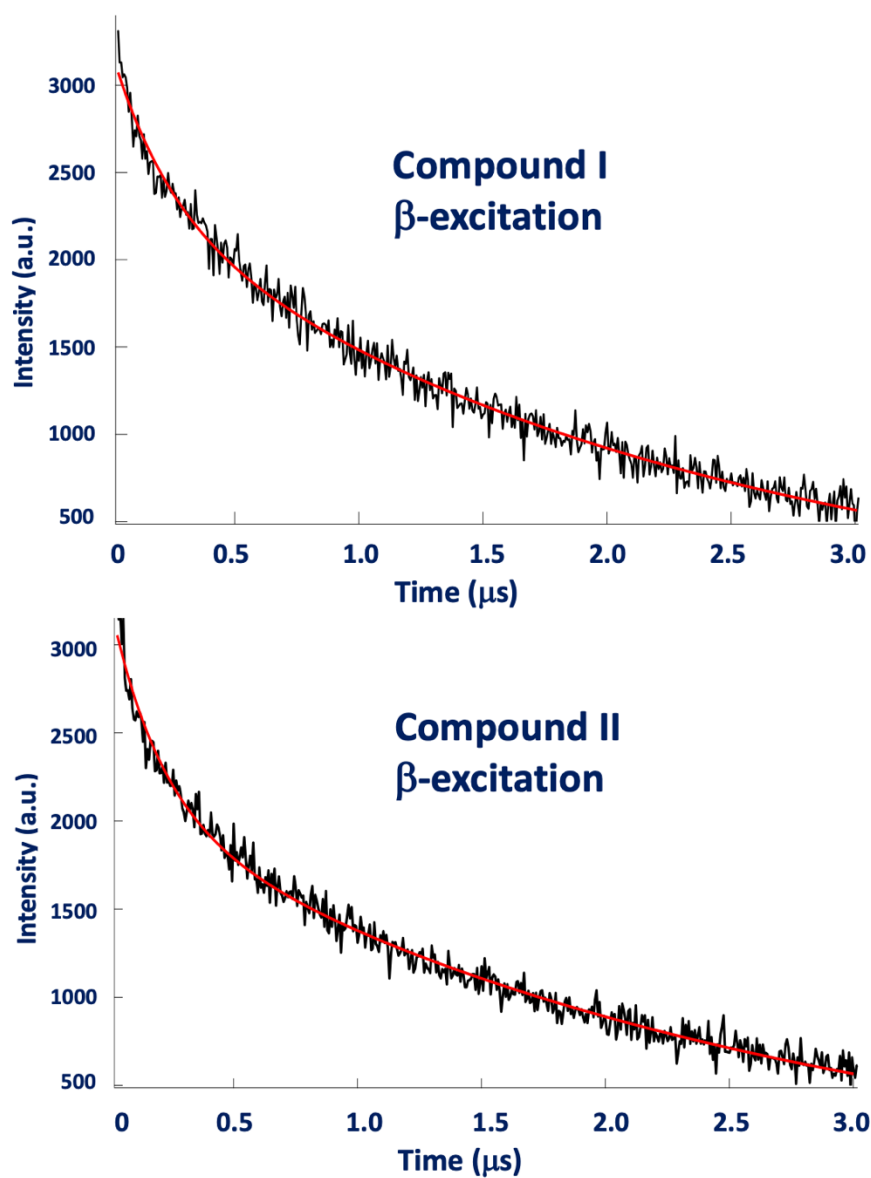


**Figure S12.** Double exponential fits ( $\text{Intensity} = I_0(A_1e^{k_1t} + A_2e^{k_2t})$ ) of scintillation responses to the  $\beta$ -ray excitation of compound **I** and **II** over the range 30 ns to 3  $\mu\text{s}$ , where  $I_0$  is the scintillation intensity at  $t = 0$ . In each case,  $k_2$  was fixed as the value derived from the fit of the emission data from 2  $\mu\text{s}$  to 7  $\mu\text{s}$  for  $\beta$ -ray excitation of the respective compounds (Figs. 6 and S9). **Top:** Compound **I**. The fit gave the values:  $A_1 = 780 \pm 27$ ,  $k_1 = 4.24 \pm 0.31 \mu\text{s}^{-1}$ ,  $A_2 = 2366 \pm 36$ , and  $k_2$  was fixed at  $0.441 \mu\text{s}^{-1}$ . **Bottom:** Compound **II**. The fit gave the values:  $A_1 = 998 \pm 24$ ,  $k_1 = 4.95 \pm 0.25 \mu\text{s}^{-1}$ ,  $A_2 = 2161 \pm 29$ , and  $k_2$  was fixed at  $0.394 \mu\text{s}^{-1}$ .

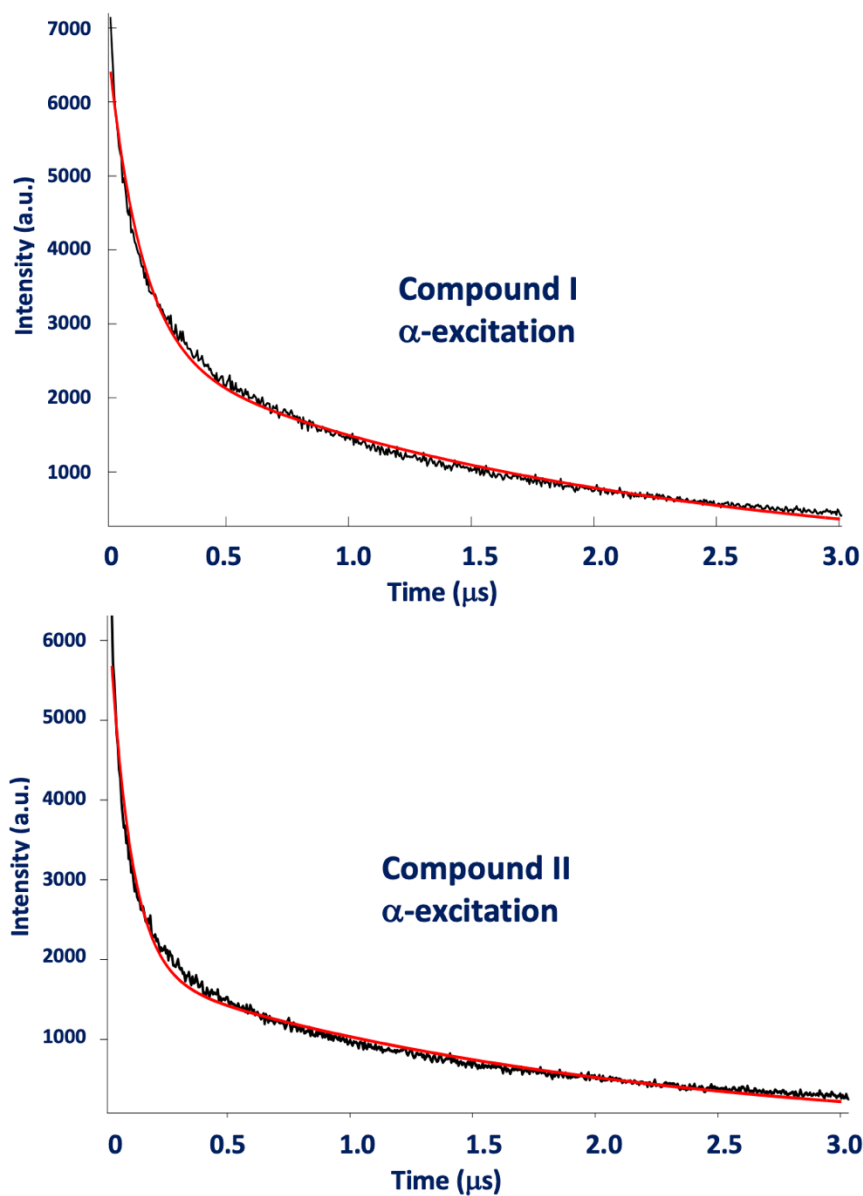
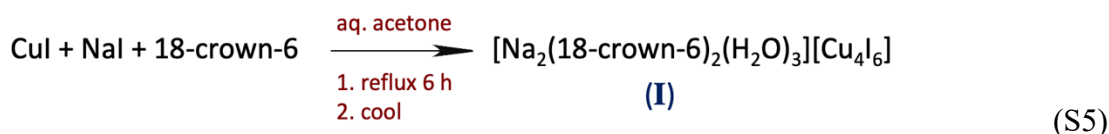


**Figure S13.** Double exponential fits ( $\text{Intensity} = I_0(A_1e^{k_1t} + A_2e^{k_2t})$ ) of scintillation responses to the alpha-particle excitation of compound **I** and **II** over the range 30 ns to 3  $\mu\text{s}$ , where  $I_0$  is the scintillation intensity at  $t = 0$ . In each case,  $k_2$  was fixed as the value derived from the fit of the emission data from 2  $\mu\text{s}$  to 7  $\mu\text{s}$  for  $\alpha$ -particle excitation of the respective compounds (Figs. 7 and S10). **Top:** Compound **I**. The fit gave the values:  $A_1 = 3773 \pm 31$ ,  $k_1 = 7.41 \pm 0.11 \mu\text{s}^{-1}$ ,  $A_2 = 2896 \pm 34$ , and  $k_2$  was fixed at  $0.517 \mu\text{s}^{-1}$ . **Bottom:** Compound **II**. The fit gave the values:  $A_1 = 3823 \pm 35$ ,  $k_1 = 11.2 \pm 0.2 \mu\text{s}^{-1}$ ,  $A_2 = 2085 \pm 19$ , and  $k_2$  was fixed at  $0.519 \mu\text{s}^{-1}$ .

## Experimental Methods:

*Materials:* The following were obtained from commercial sources: cuprous iodide (CuI, 99.95%, Aldrich), cesium carbonate (Cs<sub>2</sub>CO<sub>3</sub>, 99.9%, Aldrich), anhydrous indium (III) iodide, (InI<sub>3</sub>, 99.999%, Fisher Scientific), benzo-15-crown-5 (Alfa Aesar), 18-crown-6 (Alfa Aesar), sodium iodide (NaI, Fisher Scientific), and ascorbic acid (138 Foods Inc.).

*Synthesis of copper(I) compounds:* Compound **I** ([Na<sub>2</sub>(18-crown-6)<sub>2</sub>(H<sub>2</sub>O)<sub>3</sub>][Cu<sub>4</sub>I<sub>6</sub>]) was prepared by a procedure modified from that of Nurtaeva and Holt.<sup>1</sup> Portions of CuI (2 mmol, 0.382 g), 18-crown-6 (2 mmol, 0.528 g), NaI (3 mmol, 0.450 g) and ascorbic acid (0.213 g) were added to a solution of water (3 mL) and acetone (40 mL) and the resulting mixture was heated under reflux for 6 h until the CuI dissolves completely (eq. S5). The ascorbic acid was present to preserve the reduced oxidation state of the copper. The resulting yellow solution was filtered while hot and allowed to stand at room temperature for 3 days whereupon yellow plates and blocks were isolated by filtration.



Compound **II** ([Li(benzo-15-crown-5)<sub>2</sub>(H<sub>2</sub>O)]<sub>2</sub>[Cu<sub>4</sub>I<sub>6</sub>]) was prepared by an analogous method. A saturated solution of LiI in water (5 mL) was added to a mixture of CuI (2 mmol, 0.382 g), benzo-15-crown-5 (1.5 mmol, 0.402 g), ascorbic acid (0.213 g) and acetone (40 mL). The resulting suspension was heated under reflux until all solids had dissolved (4 h). The solution was allowed to cool slowly, and yellow plates were observed to form after slow (2 days) evaporation. The X-ray crystal structure of **II** was shown to be identical to the published structure.<sup>1</sup>

*Photophysical measurements;* Diffuse reflectance spectra were recorded for compounds **I** and **II** using a Perkin Elmer Lambda 750 Spectrometer with a Perkin Elmer 60 mm integrating sphere accessory. Luminescence and excitation spectra of solids were obtained using a Photon Technology International (PTI) spectrofluorometer with an 814 PMT detection system at 1 nm resolution. This system is equipped with a tunable excitation source.

PL emission lifetimes were measured by using the pulsed laser system in the UCSB Optical Characterization Facility (OCF). Emission transients on the long-timescale were collected using a multichannel-scaler analyzer based on the Becker and Hickl MSA-300 board. Excitation laser pulses with a duration of approximately 200 fs, wavelength 290 nm, and variable repetition rate were generated using an optical harmonic generator (Light Conversions UVVIsNIR), an optical parametric amplifier (Light Conversions TOPAS prime), and a Ti:Sapphire regenerative amplifier (Coherent Astrella). The pulse energy was controlled using a neutral density filter wheel. The luminescence was collected at 90° and focused onto the input slit of a spectrometer (Acton SP300) through a UV-blocking Schott glass filter (N-WG320). The light dispersed by the spectrometer was detected by a photon-counting PMT module (Hamamatsu H8259-02) and electric pulses were fed into the counting board along with the triggering signal from the laser controller. The IRF temporal width is less than 5 ns. Time-averaged spectra were collected with a CCD camera (Andor

iDus 401) mounted on the second spectrometer port. The spectra were corrected for the instrument response by measuring a spectrum of a calibrated radiometric light source (Ocean Optics LS-1) and corresponding correction factors.

*Radioluminescence techniques:* Radioluminescence spectra were recorded using several different methods. At UCSB the RL spectra were obtained on a custom-built apparatus by integrating the emission resulting from continuous excitation from a sample using a Cu ATPS XRD1000 X-ray tube as the excitation source (SI Fig. S14). The RL spectra were collected using an optical fiber and recorded using an Ocean Optics HR4000 high resolution spectrometer and laptop. Acquisition times were generally 30-60 s.

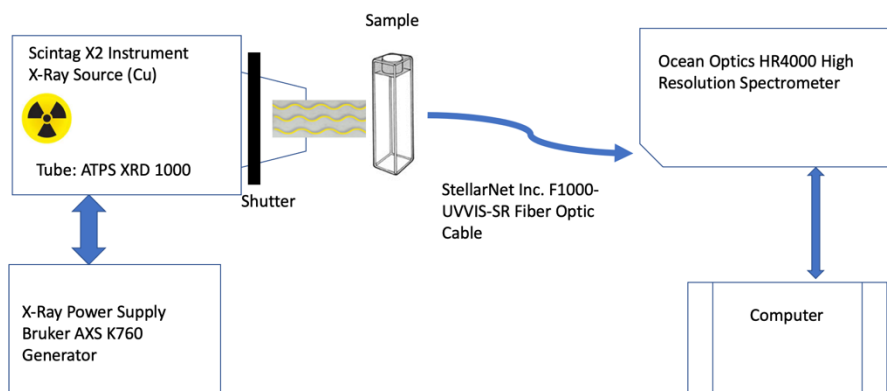


**Figure S14.** UCSB apparatus to record x-ray radioluminescence spectra using a Cu X-ray tube (40 kV, 30 mA).

TRRL spectra and lifetimes using X-ray excitation were measured using the apparatus developed at STL shown in Figure S15. The pulsed X-ray source provides a high flux of incident events with time resolution limited by the pulse width and the gated intensifier shutter response, both well-suited for TRRL spectroscopy of the materials studied here. The time-resolved X-Ray scintillation spectrometer used a Golden Engineering MR200 pulsed 150 keV X-Ray source to excite thin solid samples placed at the output. The MR200 delivers 2.5 mRad,  $\leq 60$  ns pulses at approximately 25 Hz. During pulsed X-Ray experiments, the time profile is monitored with a fast scintillator/PMT system as shown in Figure S15. There are no X-Rays emitting from the source at longer times.

A small, thin aluminum mirror was used to direct scintillation from the sample to a bare quartz 200 micron 19-fiber bundle coupled terminated at a  $\frac{1}{4}$  meter spectrograph with a slow scan intensified CCD (ICCD) detector. An RF loop was used to generate a stable trigger pulse for the microchannel plate gate circuit. The ICCD camera was gated at several exposure widths (50 ns, 1  $\mu$ s and 3  $\mu$ s). Delays from zero to as long as 30  $\mu$ s were used to capture the scintillation intensity for the entire spectrum as a function of time. The X-ray output was monitored using a fast scintillator/PMT placed in the beam with a copper attenuator. A digital scope monitored the X-ray pulse width and peak height. Typically, 75 pulses ( $\sim 180$  mRads per acquisition) were triggered per detector acquisition. Time-resolved data consisted of several collections at a sequentially longer delays at a fixed gate width. Programming of the intensifier gate width and delay were used to

generate time-resolved spectra from 380 to 750 nm which was calibrated against several pen lamps. Care was taken shield all electronics and the fiber bundle from the pulsed X-ray source.

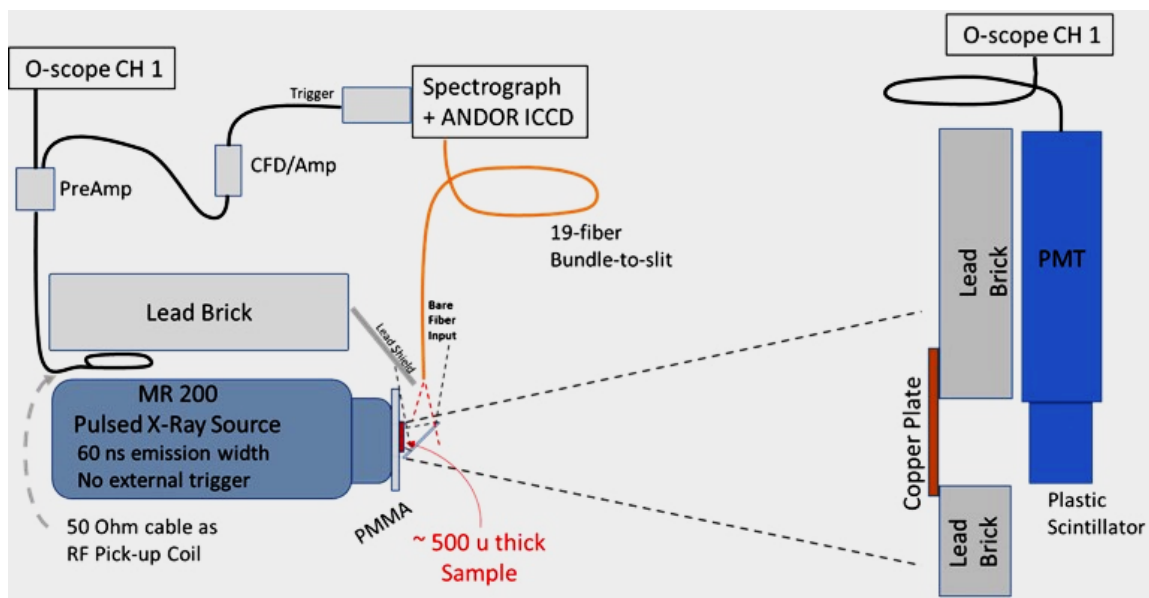


**Figure S15.** Time-resolved X-Ray scintillation spectrometer assembled for generating TRRL spectra.

A different STL instrument recorded the time-resolved scintillation triggered by  $\beta$ - and  $\alpha$ -particles. Figure S16 shows the functional block diagram of the Fluor Decay System (FDS) that was used to acquire time-resolved scintillation traces by time-correlated single photon counting (TCSPC).<sup>2-4</sup> Two different radiation sources were used. For excitation with  $\beta$ -electrons, the source was  $^{90}\text{Sr}$  (@46  $\mu\text{Ci}$ ), which  $\beta$ -decays to  $^{90}\text{Y}$  with an energy spectrum that maxes at 546 keV. The  $^{90}\text{Y}$ -90  $\beta$ -decays to  $^{90}\text{Zr}$  with energies up to 2.28 MeV. Since the  $^{90}\text{Y}$  half-life is shorter, there are equal numbers of  $\beta$ -particles from each. For excitation with  $\alpha$ -particles, the source was  $^{224}\text{Cm}$ , which emits 5.763 MeV and 5.806 MeV  $\alpha$ -particles. The capsule containing the source has a very thin stainless steel foil window designed to allow  $\alpha$ -particles to escape, albeit with some energy loss, the et energies of these being more than 3–3.5 MeV.

The FDS captures the scintillation decay on a sub-ns time scale by tagging the arrival times of single photons relative to the initial event trigger. Solid samples are placed directly in front of a fast photomultiplier tube (PMT) to generate a start pulse. The many-photon start pulse originates at the PMT signal from the scintillation event. A constant fraction discriminator (CFD) produces a highly reproducible timing fiducial that starts a time-to-amplitude converter (TAC). Each single photon detected at the microchannel plate (MCP) acts as a stop pulse. The start-stop time difference is collected on a multichannel analyzer (MCA) which generates the time versus intensity output for each event. The start rate is substantially larger than the stop rate, and corrections were made for both accidental coincidences and pile-up in the FDS data. The configuration shown is a two-scintillator system in which the TAC is started by radiation-induced flashes from a bright (500-ps FWHM) scintillator closely coupled to a 14-stage PMT. The TAC is stopped by single-photon

pulses from an amplified high-gain microchannel-plate photomultiplier viewing the sample. The experimental setup has a resolution of approximately 100 ps and can count for arbitrarily long periods so that even weak phosphorescent responses can be mapped out as a function of time, although long acquisition times for the latter may be necessary. The FDS provides TRRL response over decades of time resolution; however, the spectral information is limited by using a single optical filter PMT response.

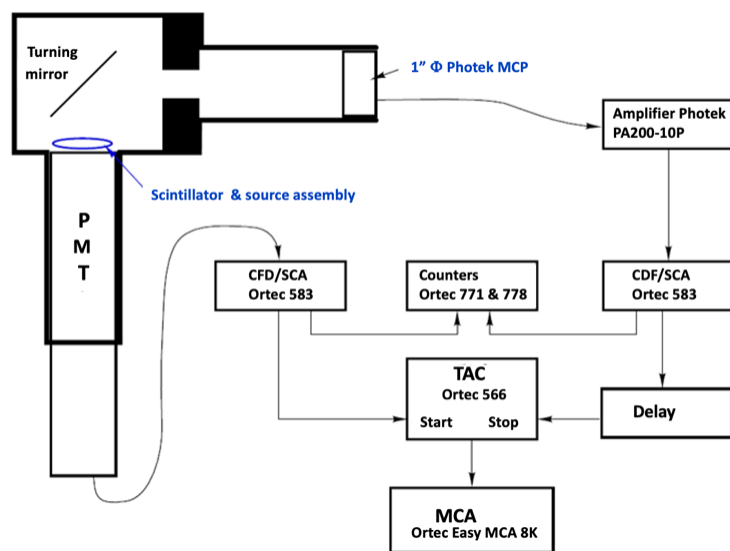


**Figure 16.** The STL Fluor Decay System based on time-correlated single photon counting (see refs 2-4).

### References:

1. A. Nurtaeva, E. M. Holt, *Acta Cryst.* 1999, **C55**, 1453-1457.
2. W. Becker, *Advanced Time-Correlated Single Photon Counting Techniques*; Springer series in chemical physics; Springer: Berlin; New York, 2005.
3. J. Flournoy, *J. Int. J. Radiat. Appl. Instrum., Part C. Rad. Phys. Chem.* 1988, **32**, 265–268.
4. V. Geppert-Kleinrath, M. S. Freeman, C. R. Hurlbut, F. Merrill, J. R. Tinsley, P. Volegov, C. Wilde, *Rev. Sci. Instrum.* 2018, **89**, 101142.